

2012-08-03

A Morphological Study of Nanomaterials and Biomolecules using Atomic Force Microscopy.

Ravi A. Patel

University of Miami, rpatel417@gmail.com

Recommended Citation

Patel, Ravi A., "A Morphological Study of Nanomaterials and Biomolecules using Atomic Force Microscopy." (2012). *Open Access Theses*. Paper 371.

http://scholarlyrepository.miami.edu/oa_theses/371

This Open access is brought to you for free and open access by the Electronic Theses and Dissertations at Scholarly Repository. It has been accepted for inclusion in Open Access Theses by an authorized administrator of Scholarly Repository. For more information, please contact jrenaud@miami.edu.

UNIVERSITY OF MIAMI

A MORPHOLOGICAL STUDY OF NANOMATERIALS AND
BIOMOLECULES USING ATOMIC FORCE MICROSCOPY

By

Ravi A. Patel

A THESIS

Submitted to the Faculty
of the University of Miami
in partial fulfillment of the requirements for
the degree of Master of Science

Coral Gables, Florida

August 2012

©2012
Ravi A. Patel
All Rights Reserved

UNIVERSITY OF MIAMI

A thesis submitted in partial fulfillment of
the requirements for the degree of
Master of Science

A MORPHOLOGICAL STUDY OF NANOMATERIALS AND
BIOMOLECULES USING ATOMIC FORCE MICROSCOPY

Ravi A. Patel

Approved:

Roger M. Leblanc, Ph.D.
Professor of Chemistry

M. Brian Blake, Ph.D.
Dean of the Graduate School

Francisco Raymo, Ph.D.
Professor of Chemistry

Burjor Captain, Ph.D.
Professor of Chemistry

Kerim M. Gattás Asfura, Ph.D.
Associate Scientist
Diabetes Research Institute
University of Miami
Miller School of Medicine

PATEL, RAVI A.

(M.S., Chemistry)

A Morphological Study of Nanomaterials
and Biomolecules using Atomic Force
Microscopy

(August 2012)

Abstract of a thesis at the University of Miami.

Thesis supervised by Professor Roger M. Leblanc.

No. of pages in text. (37)

Understanding the morphologies of molecules and particles has played a key role in understanding key concepts such as mechanisms of formation, interaction and application. In the current work, atomic force microscopy (AFM) techniques are used to emphasize the importance of topography in the field of nanomaterials and biochemistry. The intriguing relationship between graphene oxide and the copolymer Pluronic F-127 is investigated for its potential use in biological applications. Additionally, the importance of characterizing and calculating size distributions in semiconducting quantum dots as it relates to conduction efficiency is also described. AFM is similarly used in determining binding characteristics of two peptides, Pd4 (wild type), and A6 (mutant), onto a palladium surface as a means to study potential alternatives in palladium based “green” catalysis. Finally, the study of human insulin amyloid fibril formation is reported as a means to elucidate potential mechanisms in the growth of pathological, extracellular and insoluble protein deposits that have been linked to many disease states. AFM has proven to be an invaluable technique to study morphology in the realm of nanomaterials and biomolecules.

Acknowledgements

My utmost gratitude and thanks go to my research supervisor, Dr. R. M. Leblanc for being more than just a great mentor and advisor. He was a remarkable friend who would always have the time to listen and talk about my problems and concerns.

I would like to thank my committee: Dr. B. Captain and Dr. F. Raymo for their valuable insight and advice during the past few years. I would also like to extend my appreciations to Dr. K. Gattàs-Asfura for his time, advice and help.

I would like to thank everyone in the Department of Chemistry for their help during the past years, especially Sara Sucklal, Lydia Gonzalez, Susana Gadanyi, Juanita Hernandez and Raul Hernandez.

I would like to thank my fellow graduate students and friends, both current and past, at the University of Miami who have made my time here very special. I extend a special acknowledgement to Anup Dadlani, Nicholas Crawford, Shanghao Li, Sheba Johnson and Dr. J. Orbulescu, for their endless help, advice and friendship.

Finally, I would like to thank my family for their unconditional support and love through all of my trials, tribulations and triumphs here at the University of Miami.

Table of Contents

| | |
|--|-----------|
| List of Figures..... | vi |
| Chapter 1. Introduction..... | 1 |
| 1.1 History of AFM..... | 1 |
| 1.2 Principles..... | 2 |
| 1.3 Components | 3 |
| 1.3.1 Probe..... | 3 |
| 1.3.2 Piezo-crystal Scanner | 3 |
| 1.3.3 Detector | 4 |
| 1.4 Methodology of AFM..... | 4 |
| 1.4.1 Contact Mode | 4 |
| 1.4.2 AC Mode | 5 |
| 1.4.3 Phase Contrast Imaging..... | 7 |
| 1.5 Selected Applications | 7 |
| 1.5.1 Imaging nanomaterials | 7 |
| 1.5.2 Biomolecule imaging..... | 9 |
| Chapter 2. Materials and Methods..... | 10 |
| 2.1 Chemicals | 10 |
| 2.2 Substrates..... | 10 |
| 2.2.1 Mica | 11 |
| 2.2.2 Silicon..... | 12 |
| 2.2.3 Graphite | 13 |
| 2.2.4 Gold | 13 |
| 2.4 Preparation of peptide binding..... | 14 |
| 2.4.1 Preparation of the substrate | 14 |
| 2.4.2 Methodology of QCM | 14 |

| | |
|---|-----------|
| 2.4.3 Deposition of peptide..... | 15 |
| 2.5 Preparation of fibrils..... | 15 |
| 2.5.1 Human insulin..... | 15 |
| Chapter 3. Nanomaterials | 16 |
| 3.1 Pluronic F-127 | 16 |
| 3.1.1 Background..... | 16 |
| 3.1.2 Self-assembly of Pluronic F-127 | 16 |
| 3.2 Graphene oxide..... | 18 |
| 3.2.1 Background..... | 18 |
| 3.2.2 Aggregation of GO in electrolyte solution | 19 |
| 3.2.3 Interaction between GO and Pluronic F-127 | 20 |
| 3.3 (ZnS)-CdSe quantum dots | 22 |
| 3.3.1 Background..... | 22 |
| 3.3.2 Size characterization..... | 23 |
| 3.3.3 Size histogram | 24 |
| Chapter 4. Peptide Binding | 26 |
| 4.1 Background..... | 26 |
| 4.2 Nature of binding | 27 |
| Chapter 5. Amyloid Fibril Formation..... | 31 |
| 5.1 Background..... | 31 |
| 5.2 Human Insulin..... | 31 |
| Chapter 6. Future Work..... | 35 |
| References | 36 |

List of Figures

| | |
|--|----|
| Figure 1.1 Visual representations of principles behind scanning tunneling microscopy (A) and atomic force microscopy (B). ⁴ | 2 |
| Figure 1.2 Detector assembly, top view (left) and bottom view (right). ⁴ | 4 |
| Figure 1.3 Zones of interaction as tip approaches sample surface in AC mode AFM. ⁴ | 6 |
| Figure 1.4 An AFM topographic image of Al ₂ O ₃ on mica (left) and its corresponding size distribution histogram (right). ¹¹ | 8 |
| Figure 2.1 Topography and profile extraction analysis of freshly cleaved mica substrate. | 12 |
| Figure 2.2 Topography and profile extraction analysis of cleaned silicon wafer substrate. | 12 |
| Figure 2.3 Topography and profile extraction analysis of cleaned gold substrate | 14 |
| Figure 3.1 Molecular formula of Pluronic F-127 copolymer, where x = 101, y = 56 and z = 101. ²⁶ | 16 |
| Figure 3.2 Self-assembly of Pluronic F-127 deposited on (A) mica and (B) HOPG. | 17 |
| Figure 3.3 Profile extraction analysis of Pluronic F-127 deposited on mica. | 17 |
| Figure 3.4 Profile extraction analysis of Pluronic F-127 deposited on HOPG. | 18 |
| Figure 3.5 Profile extraction analysis of GO. | 18 |
| Figure 3.6 2D images of graphene oxide (A) topography and (B) phase contrast. | 19 |
| Figure 3.7 2D topography (A) and phase contrast (B) of a 2:1 solution of GO to Pluronic F-127. | 20 |
| Figure 3.8 Profile extraction analysis of GO / Pluronic F-127 mixture (2:1). GO (A), GO / Pluronic F-127 interaction (B). | 21 |

| | |
|---|----|
| Figure 3.9 3D topography of GO / Pluronic F-127 mixture (2:1)..... | 22 |
| Figure 3.10 2D (a) and 3D (b) topography images of (ZnS)-capped CdSe quantum dots. | 24 |
| Figure 3.11 Profile extraction analysis of (ZnS)-capped CdSe quantum dots..... | 24 |
| Figure 3.12 Histogram of quantum dot sizes derived from AFM imaging..... | 25 |
| Figure 4.1 Topography and phase contrast of clean QCM substrate..... | 27 |
| Figure 4.2 2D (A) and 3D (B) topography and phase contrast (C) of palladium coated chip after control QCM experiment..... | 28 |
| Figure 4.3 Topography of Pd4 (top) and A6 (bottom) peptides at varying concentrations: (A,D) 5 $\mu\text{g/ml}$, (B,E) 10 $\mu\text{g/ml}$, (C,F) 15 $\mu\text{g/ml}$ | 29 |
| Figure 4.4 Phase contrast images of Pd4 (top) and A6 (bottom) peptides at varying concentrations: (A,D) 5 $\mu\text{g/ml}$, (B,E) 10 $\mu\text{g/ml}$, (C,F) 15 $\mu\text{g/ml}$ | 29 |
| Figure 4.5 Profile extraction analysis of Pd4 peptide at 15 $\mu\text{g/ml}$ taken with phase contrast AFM. | 30 |
| Figure 5.1 Topography of human insulin after 0 (A), 5 (B) and 10 h (C) incubation on mica..... | 32 |
| Figure 5.2 Topography of human insulin after 14 (A), 17 (B) and 20 h (C) incubation on mica..... | 33 |
| Figure 5.3 2D (A) and 3D (B) topography of human insulin after incubation for 24 h... | 34 |
| Figure 5.4 Profile extraction analysis of human insulin fibrils after 24 h incubation..... | 34 |

Chapter 1. Introduction

1.1 History of AFM

Atomic force microscopy is a technique used to visualize any molecules that are chemically or physically adsorbed onto a solid substrate. The atomic force microscope was developed in 1986 by Binnig, Quate and Gerber at Stanford University.¹ These biologists were concerned with measuring ultra-small forces on particles as small as a single atom. Previously, this could only be accomplished using Scanning Tunneling Microscopy (STM), a technology also developed by Binnig five years previously.² It is a technique for which he and his colleague H. Rohrer would win the Noble Prize for inventing. Both techniques are members of the family known as scanning probe microscopy (SPM). STM is based on the principles of quantum tunneling, whereby a particle tunnels through a barrier via non-classical mechanics. In STM, a conductive tip is brought near the surface, a voltage bias is applied allowing electrons to tunnel through the vacuum between the two, and the resulting tunneling current is recorded as a function of the tip position.³ However, a major limiting factor in using STM is that the sample must be electronically conductive. The result is that any nonconductive samples, principally biological samples, could not be imaged using STM. In order to overcome this limitation, Binnig and his co-workers created a paradigm in which the atomic forces between the probing tip and the sample surface is measured as opposed to the tunneling current; they called the technique Atomic Force Microscopy (AFM).¹

1.2 Principles

The basic principles of AFM start with a probing tip which is attached to a cantilever spring. As the tip moves laterally, in the x and y directions, a force between it and the sample deflects the cantilever, which in turn deflects the laser beam. The resulting deflection is then collected by a photodetector and then translated in to the z-movement of the piezo. This information is calculated as a function of the lateral tip position giving a three dimensional topographic image. AFM remains a non-destructive imaging technique by taking advantage of forces smaller than the interaction between two covalently bonded atoms, i.e. 10^{-9} N. A typical atomic force microscope is capable of measuring forces as small as 10^{-11} N.⁴ However, in addition to imaging, AFM has proven to be an effective means to study other properties, such as binding energies by using force curves, as well as to study surface hardness, adhesion, friction and more by utilizing phase contrast imaging. The principles of phase contrast AFM will be discussed later. Additionally, because AFM is based on measuring the forces between the tip and sample, it can also be used as an exquisite sensor for molecular forces, such as hydrogen bonding, van der Waals interactions and electrostatic forces. Figure 1.1 visually depicts the basic principles involved in both STM and AFM techniques.

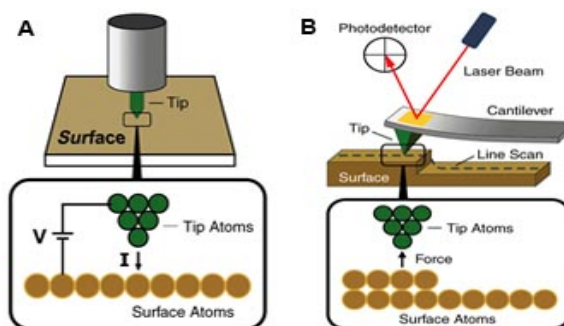


Figure 1.1 Visual representations of principles behind scanning tunneling microscopy (A) and atomic force microscopy (B).⁴

1.3 Components

1.3.1 Probe

The probe represents the cantilever with a sharp tip attached at one end. Cantilevers are machined out of either silicon or silicon nitride and are made in two shapes, V-shaped and rectangular. They typically range from 100 to 200 micrometers in length, 10 to 40 micrometers in width and 0.3 to 2.0 micrometers in thickness, and have a spring constant range of 0.001 to 100 N/m. Integrated cantilevers are characterized by their force constant and resonant frequency and vary depending on application, type of sample surface, imaging environment, and type of image being generated. The tip generally has a nominal radius of < 10 nm, however much sharper tips are commercially available. It is the tip that interacts with the sample surface, therefore the advantages of sharper tips is a direct increase in image resolution. Tip geometries also vary and may include tetrahedral, pyramidal, or conical.

1.3.2 Piezo-crystal Scanner

Piezocrystals are ceramic materials that expand and contract in the presence of a voltage differential; this is called the piezoelectric effect which was first discovered and demonstrated by brothers Jacques and Pierre Curie in 1880.⁵ These materials can also develop an electrical potential in response to mechanical pressure, this is known as the reverse piezo effect. It is due to the piezocrystals that movements in the x, y, and z direction are possible. These components as well as the cantilever assemblies are situated in what is called the scanner. Multiple scanner types are available, small multi-purpose scanners provide up to 125 square microns of coverage whereas large multi-purpose

scanners can provide up to 8100 square microns of coverage. The latter is also available with closed-loop positioning in order to achieve ultra-precise positioning by eliminating noise.

1.3.3 Detector

The quadrilateral photodiode detector is what is used to receive the reflected laser beam off the back of the cantilever as it scans the sample surface. The top and bottom halves of the detector monitor deflection for AFM imaging whereas the right and left halves report twisting of the cantilever for lateral force imaging. AFM detectors are engineered to be extremely sensitive to minute deflections in order to maintain a high degree of precision.

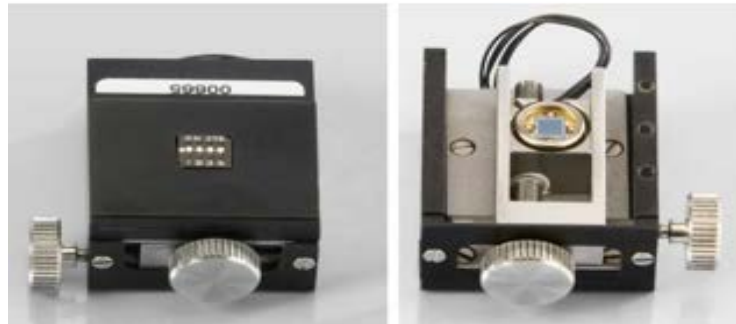


Figure 1.2 Detector assembly, top view (left) and bottom view (right).⁴

1.4 Methodology of AFM

1.4.1 Contact Mode

One of the most common modes utilized in imaging Atomic Force Microscopy is Contact Mode. In Contact Mode, the tip is slowly lowered close to the sample to a set point predefined by the user. The sample is then scanned by rastering the tip across the surface. The laser beam aimed at the back of the cantilever detects changes in the deflection. The AFM tip must be attached to a cantilever with a very low spring constant

(0.0001 - 5 N/m) so that it easily deflects when exposed to contact forces due to tip-sample repulsion, these forces range from 0.1-1000 nN.⁴ AFM in Contact Mode can be performed in two modes, constant height or constant force, both modes utilize Hooke's Law, $F = -k \cdot \Delta x$, where F is the repulsive force, k is the cantilever spring constant, and Δx is the cantilever deflection.

In constant height mode, the probe scans the surface at a constant height and the tip deflection is recorded to give topography as a function of lateral position. This mode is typically used to image relatively flat surfaces. In constant force mode, the repulsive force between the tip and sample surface is kept constant due to a feedback loop controlling the z-axis motion of the piezo. This movement is then recorded and graphed to give a topographic image.

The advantages of Contact Mode include high scan speeds and "atomic resolution". However, the lateral forces caused by the rastering of the tip can distort the images, especially when scanning a softer sample such as DNA or proteins. Additionally, when imaging in air, capillary forces from a deposited fluid layer may cause large normal forces, introducing undesired artifacts. To overcome this limitation, when possible, Contact Mode AFM is typically performed in liquid phase.

1.4.2 AC Mode

A newer approach that does not involve raster scanning of the surface is AC Mode. To perform a scan using this mode, the cantilever is oscillated at its resonant frequency, resulting in sinusoidal motion in the z-direction. In AC Mode, when the tip encounters changes in the elevation of the sample, the amplitude of the oscillation

changes. In this situation, the feedback mechanism acts to keep constant amplitude, the set point value. The topography image is then generated by utilizing the voltage needed to move the z-position piezo actuator, which is multiplied with the piezo sensitivity given in nanometer/volt. Two subtypes of imaging have been derived from AC Mode, Noncontact, also called Attractive Mode due to net interactions being in the attractive regime of the potential curve, and Intermittent, or Tapping Mode, which lies in the repulsive regime.

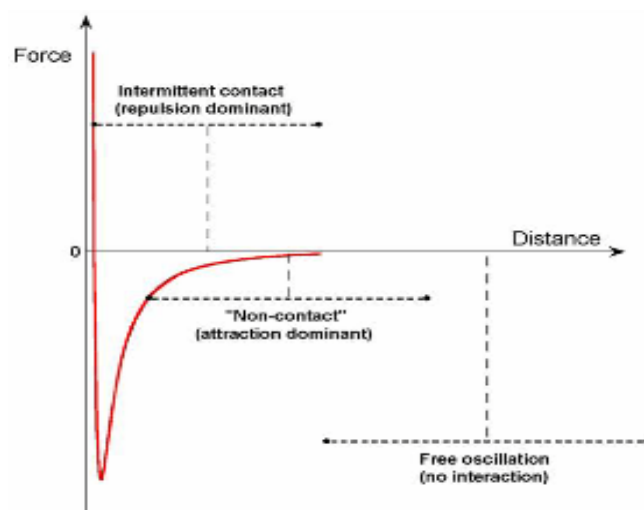


Figure 1.3 Zones of interaction as tip approaches sample surface in AC mode AFM.⁴

Noncontact Mode relies on forces between the tip and the sample to affect oscillation, whereas Tapping Mode physically touches the surface at the bottom of the oscillation. Due to close approaches to the surface, cantilevers with stiff spring constants, typically between 20 - 100 N/m, are used to avoid sticking with the sample. Advantages of AC Mode in general include higher lateral resolution (1-5 nm) and no lateral forces leading to less damage upon softer samples, making AC Mode an ideal candidate to image biological samples. However, unlike Contact Mode, AC Mode is often performed in air or gas as opposed to liquid due to dampening of the cantilever amplitude.

Nevertheless, novel approaches of Tapping Mode AFM performed in fluids have been studied.

1.4.3 Phase Contrast Imaging

Phase contrast AFM is a powerful surface characterization tool that can be used as an alternative or supplement to topographic imaging. The advantage of phase contrast over spatial topography is that the images are scanned by detecting the viscoelasticity dissipation of the surface and may reveal more substantial characteristics versus the corresponding topographic image. It becomes increasingly useful when imaging non-flat surfaces on which samples with small details may not be noticeable with traditional topographic methods.⁶ Phase contrast AFM functions by monitoring the phase lag on the oscillation of the cantilever, the difference between the nominal and experimental frequency is recorded and displayed in units of degrees.⁷ The greater the phase lag, the brighter the pixels appear on the image, and visa-versa. Chemical and physical properties of the material surfaces affect the dampening of the tip frequency; this includes but is not limited to elasticity, friction and adhesion.^{8,9} Because the tip oscillation is being monitored, Tapping Mode AFM must be used in order obtain a phase contrast image, however both phase and topography can be recorded simultaneously.

1.5 Selected Applications

1.5.1 Imaging nanomaterials

Nanomaterials have become the focus of an enormous amount of research over the past decade. One might argue that the ongoing quest for miniaturization, leading to the discovery and progression of AFM, has led to the acceleration in nanotechnology research. These nanomaterials, whether developed through a top-down method (reducing

bulk materials in size to the nanoscale), or bottom-up approach (larger materials are built up atom by atom or molecule by molecule), have broken physical barrier. In other words, materials in this size regime no longer follow the standard laws of physics; instead they behave based on ‘quantum effects’.

Materials reduced to the nanoscale present radically different behavior compared to their bulk counterparts, i.e. copper goes from opaque to transparent, palladium goes from inert to catalytic and insulators, such as silicon, become conductors.¹⁰ Furthermore, it becomes increasingly important to be able to accurately characterize the sizes of nanomaterials as that information play a crucial role in their applications. For example, as nanoparticles decrease in size, the surface area to volume ratio increases, making smaller particles more desirable for fields such as interface science. Therefore, having the ability to precisely measure nanomaterials in three-dimensions becomes a matter of improving efficiency in potential applications.

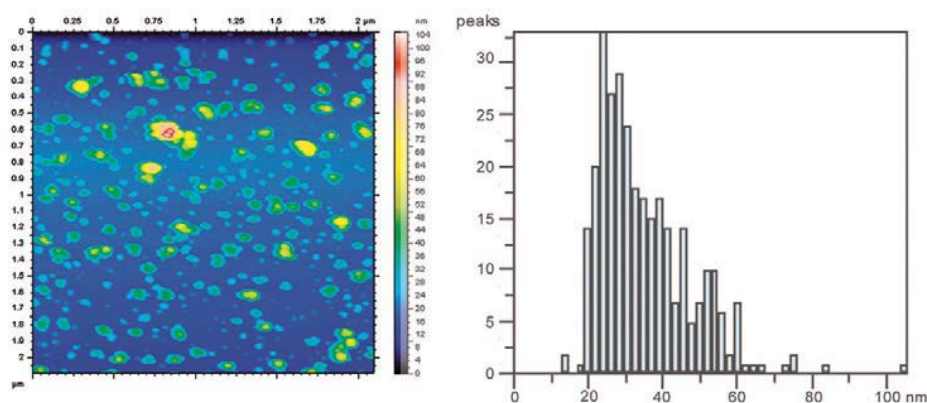


Figure 1.4 An AFM topographic image of Al₂O₃ on mica (left) and its corresponding size distribution histogram (right).¹¹

Figure 1.4, provided by Agilent Technologies, depicts how AFM is capable of characterizing alumina, or aluminum oxide, by providing a 2D topographic image which is then used to calculate the size distribution plotted in a histogram.

1.5.2 Biomolecule imaging

The AFM is very well suited for biological applications, it requires no staining of the sample, it works in air and liquid and it can provide detailed information regarding biochemical processes. As Binnig and his co-workers were biologists, it is apparent that their primary concern in developing the AFM technique was to be able to image biological samples, a feature STM did not provide. Currently, multiple techniques outside of scanning force microscopy exist to image biomolecules, particularly, electron microscopy, X-ray diffraction, nuclear magnetic resonance, and infrared spectroscopy, to an extent. However, these techniques do not allow for simultaneous study of structure and function, much like AFM does.

Large numbers of various biological samples, such as cells and cell compartments, as well as biomolecules, such as DNA and RNA have been studied with AFM. In some cases, AFM is used solely as a topographic aid, in others it is used to measure the dynamics of non-fixed materials in aqueous environments. Soon after the discovery of AFM, Drake *et al.* demonstrated the possibility of imaging proteins in an aqueous environment, this spurred further investigation which lead to Hoh *et al.* to study gap junctions between cells by using the topographic technique.^{12,13} In 2007, de Jager and van Noort suggested that unique characteristics regarding the mechanism and function of DNA and RNA in the metabolism of proteins can be determined by quantification of the number, volume, position, and shape of proteins on their substrates, this can all be obtained by using AFM.¹⁴

Chapter 2. Materials and Methods

2.1 Chemicals

Graphene oxide was provided by ACS Material LLC. Human Insulin was purchased from MP Biomedicals LLC. (Solon, OH). Pluronic F-127 was purchased from Sigma Aldrich (St. Louis, MO). ZnS capped CdSe quantum dots were graciously provided by eBioScience (San Diego, CA). The water used was purified with a Modulab 2020 water purification system from Continental Water Systems Corp (San Antonio, TX). The purified water had a specific resistance of $18 \text{ M}\Omega\cdot\text{cm}$ and surface tension of 72.6 mN m^{-1} at $20.5 \pm 0.5 \text{ }^\circ\text{C}$. Samples of GO and Pluronic F-127 were prepared by injecting $5 \text{ }\mu\text{l}$ of 0.16 mg/ml aqueous solution onto freshly cleaved mica and allowed to dry in ambient environment. Samples of ZnS capped CdSe quantum dots were prepared by placing a $10 \text{ }\mu\text{l}$ droplet of a 0.1 mM aqueous solution onto a cleaned silicon wafer substrate and allowed air dry in the ambient clean room atmosphere.

All of the AFM images were taken using an Agilent 5420 AFM instrument. The AFM is situated in a clean room (class 1000) which is regulated for temperature at $18.0 \pm 0.1 \text{ }^\circ\text{C}$ and humidity at $45 \pm 1\%$. The air in the clean room is circulated through HEPA filters. All experiments reported herein utilized AC Mode AFM to eliminate lateral force as a cause of artifacts in the images. The cantilever had a resonance frequency of 145 kHz . All images were taken at a resolution of 512×512 points per line at a speed of 0.7 lines per second.

2.2 Substrates

Since AFM images sample surfaces, the sample is very often supported on a substrate. Typically, these substrates are incredibly flat and must be extremely clean to

avoid artifacts and to improve resolution of the images. Herein, mica, silicon, graphite and gold will be discussed. Glass will not be considered due to its relatively rough surface, making it only appropriate when studying very large samples such as cells or cell organelles.

2.2.1 Mica

Mica is one of the most commonly used substrates in AFM. It is a non-conductive layered material which is cheap and easily cleaved, usually with a piece of Scotch tape. Cleaving the mica produces an atomically flat and clean surface. The most widely used form of mica is called Muscovite, $K_2Al_4Si_6Al_2O_{20}(OH,F)_4$. On a clean and freshly cleaved piece of mica, the minimum step height observed is 1 nm, which is the thickness of an individual layer.¹⁵ It has a root-mean-square roughness of 0.06 ± 0.01 nm. Additionally, the crystalline structure of mica can be used for calibration by utilizing the hexagonal lattice constant of 0.52 nm.¹⁶ Due to the large amount of surface ionization and charge on mica, it is very hydrophilic and is always covered by a thin layer of water when exposed to the ambient atmosphere. Mica has been used successfully to image biomacromolecules such as DNA and proteins.¹⁷ The adsorption of these analytes on the surface is still not very well understood, however it can be assumed that electrostatic interactions play a large role in orienting the sample onto the surface of the mica.

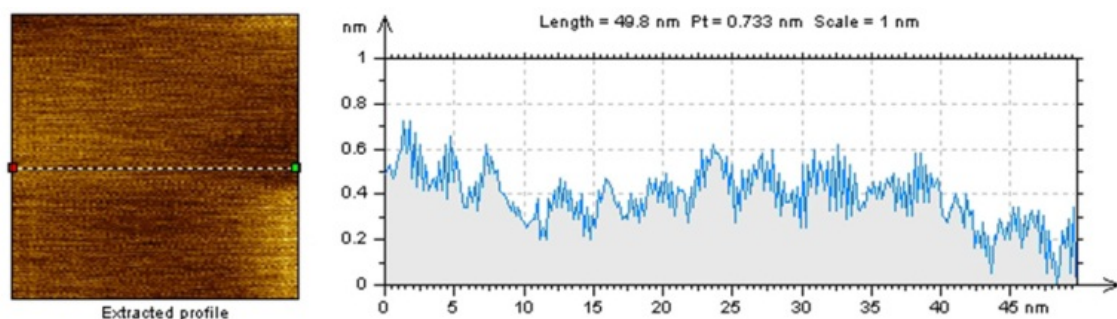


Figure 2.1 Topography and profile extraction analysis of freshly cleaved mica substrate.

2.2.2 Silicon

Silicon wafers are traditionally used in the semiconductor and optical industries. The silicon that is used by manufacturers of semiconductors is produced by removing the oxygen from silicon dioxide, purifying it, and growing it into a large crystal of pure silicon. The crystal is then cut into small slices, roughly 0.5 mm; this final product is known as silicon wafers.¹⁸ The surface of silicon wafers has a thin oxide layer which makes them hydrophilic due to surface hydroxyl groups.

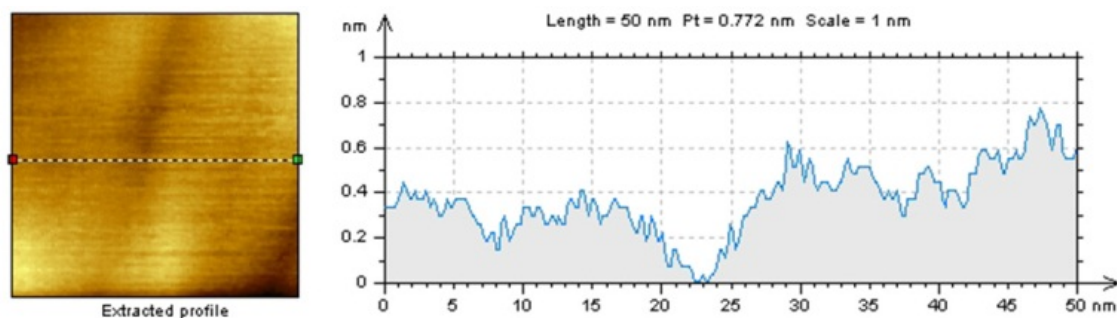


Figure 2.2 Topography and profile extraction analysis of cleaned silicon wafer substrate.

Based on the profile extraction analysis of silicon, the surface roughness and minimum step heights are comparable to mica. One may prefer using a silicon wafer substrate as the surface is consistently smooth compared to mica in which artifacts may be present due to improper cleavage. However, silicon is more expensive and may deteriorate over time due to the cleaning process.

2.2.3 Graphite

Highly ordered pyrolytic graphite (HOPG) is not as widely used as an AFM substrate. HOPG is a layered and planar structured group of sp^2 hybridized carbon rings. The surface atoms form a hexagonal lattice with a separation of 0.142 nm.¹⁹ This structure gives HOPG the property of being conductive, which is why it is more commonly used for STM measurements as conductivity is a precursor for the STM technique. Due to the surface carbon rings, HOPG is a very hydrophobic substrate. This characteristic may be responsible for poor adsorption of biological specimens. HOPG is cleaved in a similar fashion to mica as was mentioned above. Additionally, each layer is very fragile and prone to tearing and flaking, therefore artifacts from this fine structure are very common and may be confused for specimen. However, for hydrophobic samples, HOPG is primarily used as other atomically flat hydrophobic surfaces are fairly scarce.

2.2.4 Gold

Gold substrates can be made by vapor coating mica, silicon, or glass with the metal; they can also be grown epitaxial methods. Shao *et al.* describe a method to prepare an Au(111) surface in the latter technique.²⁰ Gold surfaces are beneficial in that gold is chemically inert against oxygen and is also stable against radicals. Additionally, it binds organic thiols as well as disulfides with high efficiency which can be advantageous when imaging biological samples.²¹ Based on Figure 2.3, the surface of a gold substrate is extremely flat making it a suitable option for smaller biological specimens. However,

gold may not be appropriate for all samples as many molecules tend to have an affinity for the metal, which may distort the native conformations thereby producing artificial images.

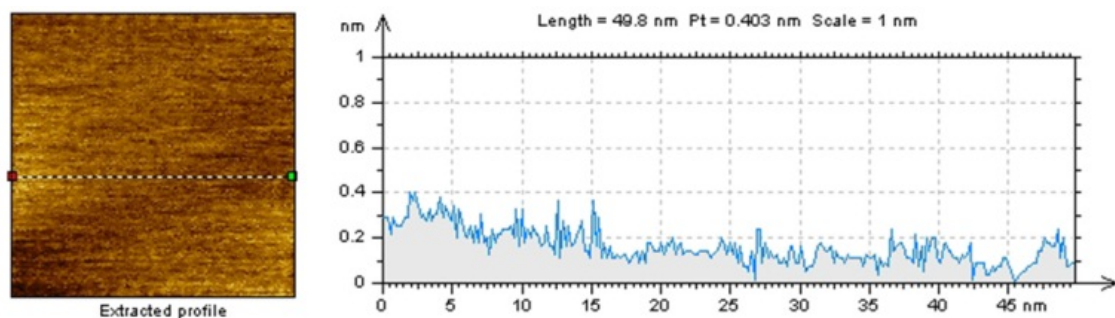


Figure 2.3 Topography and profile extraction analysis of cleaned gold substrate .

2.4 Preparation of peptide binding

2.4.1 Preparation of the substrate

The first step towards studying the behavior of peptide binding is preparation of the substrate. In the experiments reported herein, gold coated quartz crystal microbalance (QCM) chips were initially obtained and sputter coated with palladium. The particular facet of Pd, that has been proven to interact with the peptides in question, was chosen based on adsorption studies performed previously. Upon deposition, the chips were cleaned by using a strong base bath and UV radiation. AFM reference images of the cleaned substrates were then taken as a control.

2.4.2 Methodology of QCM

Quartz crystal microbalance is a technique that is used to study the adsorption of various molecules, such as proteins and self-assembled monolayer constructs, either in the gas or solution phase.^{22,23} In a typical QCM experiment, a quartz crystal is mechanically excited into resonance by applying an alternating potential to conducting films located on either side of the crystal. As the chip is being resonated, the analyte is

being fed onto the surface via a flow-through system. The oscillating frequency is sensitive to the amount of adsorbed materials onto the crystal surface; this is used to monitor the deposition of thin-film materials or molecules.

2.4.3 Deposition of peptide

Two peptides were selected to be studied, Pd4, which is the wild type, and A6, the mutant. Pd4 is a twelve amino acid peptide that has been shown to bind palladium via a phage display combinatorial library.²⁴ A single histidine residue at position six has been substituted for an alanine residue in the mutant A6 peptide. Three peptide concentrations were used to perform the QCM adsorption experiments, 5, 10 and 15 $\mu\text{g/ml}$, which totals to six samples. A flow of ultrapure water followed after peptide administration to remove any excess unbound peptide. After each deposition, the crystals were dried with a soft stream of nitrogen. Each sample was imaged without further preparation using AC mode AFM for topography and phase contrast.

2.5 Preparation of fibrils

2.5.1 Human insulin

Fresh solutions of human insulin were prepared at 0.1 wt.% (0.17 mM) at a pH of 2, adjusted by addition of HCl. Samples were incubated at 65°C for 0 min, 5, 10, 14, 17, 20 and 24 h, in accordance to literature.²⁵ Immediately after incubation, the samples were diluted 200 times using ultrapure water which had been adjusted to pH 2 with HCl. 20 μl of the diluted insulin samples were then deposited onto freshly cleaved mica. The sample slides were then allowed to dry in ambient atmosphere and then imaged using AC mode AFM.

Chapter 3. Nanomaterials

3.1 Pluronic F-127

3.1.1 Background

Pluronic F-127 (generic name, poloxamer 407) is a hydrophilic nonionic surfactant polyol which has an approximate molecular weight of 12,000 Da. The copolymer is composed of three blocks, a central hydrophobic block consisting of polypropylene glycol (PPG), surrounded by two hydrophilic blocks of polyethylene glycol (PEG).²⁶ The two PEG blocks are approximately 101 repeated units whereas the polypropylene glycol is roughly 56 repeated units. Pluronic F-127 has been previously shown to facilitate the solubilization of water-insoluble materials such as dyes and other physiological compounds.²⁷

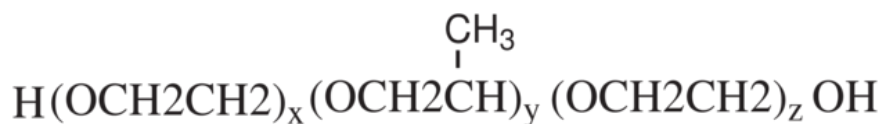


Figure 3.1 Molecular formula of Pluronic F-127 copolymer, where $x = 101$, $y = 56$ and $z = 101$.²⁶

3.1.2 Self-assembly of Pluronic F-127

Pluronic F-127 has been known to self-assemble in solution. The mechanism of self-assembly in this block co-polymer is still rather unknown. However, based on the AFM images presented herein, a hydrophobic interaction-based mechanism can be hypothesized. Additionally, it is apparent that substrate properties have a strong influence on the morphology of the self-assembled polymer strings.

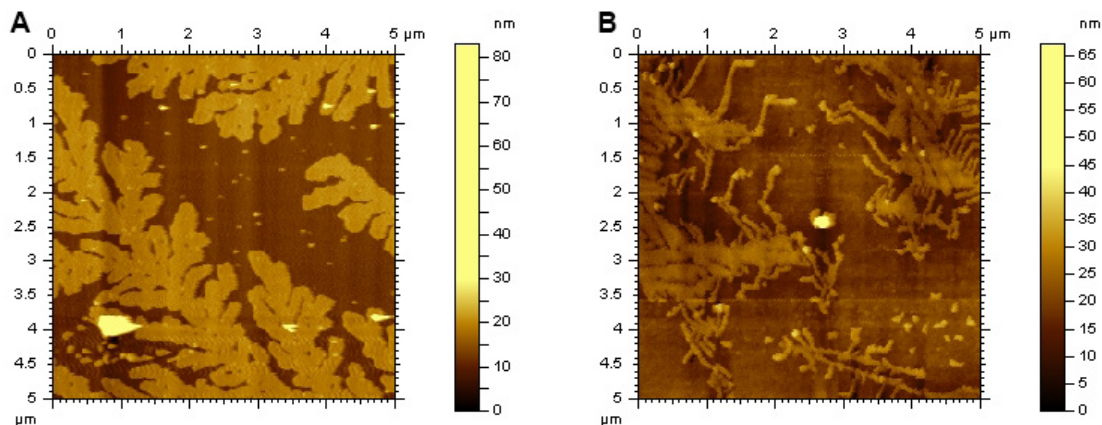


Figure 3.2 Self-assembly of Pluronic F-127 deposited on (A) mica and (B) HOPG.

It is clearly seen that on a hydrophilic surface such as mica, the two hydrophilic PEG ‘wings’ (segments ‘x’ and ‘z’ in Figure 3.1) of Pluronic F-127 lay flat and self-assembly occurs as the hydrophobic PPG central segments of the copolymer begin to line up together, resulting in a flatter and shorter morphology (See Figure 3.3). Whereas on a hydrophobic surface such as HOPG, the two ‘wings’ are repelled off the surface and remain elevated in air, giving the self-assembly a narrower and taller morphology (See Figure 3.4). Based on the profile extraction analysis in Figure 3.3, one can assume that the Pluronic F-127 seen imaged is double layered based on 5 nm heights found in the literature.²⁸



Figure 3.3 Profile extraction analysis of Pluronic F-127 deposited on mica.

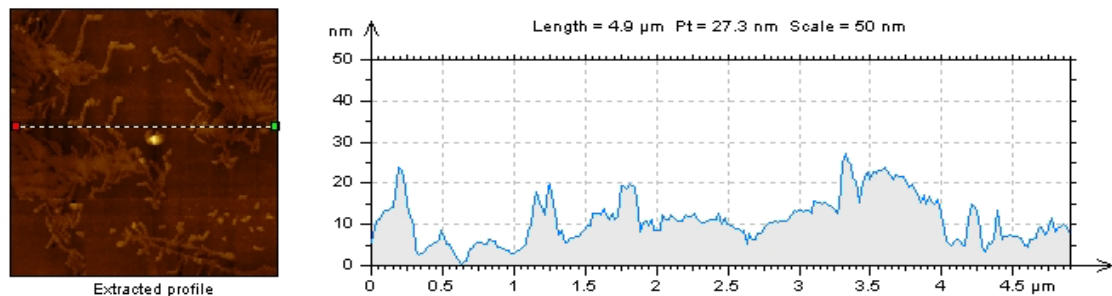


Figure 3.4 Profile extraction analysis of Pluronic F-127 deposited on HOPG.

3.2 Graphene oxide

3.2.1 Background

A relatively new nanomaterial that has taken the field by storm is graphene oxide (GO). GO is a two-dimensional carbon based nanomaterial which includes functional groups, such as carboxylic acid groups along the edges, phenol hydroxyl and epoxide groups on the basal plane.²⁹ GO provides various advantages over other nanomaterials such as large surface interface, high water solubility, and great biocompatibility. Graphene is most commonly synthesized by reacting pure graphite powder with very strong oxidizing agents such as KMnO_4 in concentrated sulfuric acid. The graphene sheets are then derivatized with carboxylic acids, phenyl hydroxides and epoxides to yield GO.³⁰ GO is characterized by two very different length scales. The thickness of a single sheet of GO is reported to be 1 nm (Figure 3.5).³¹

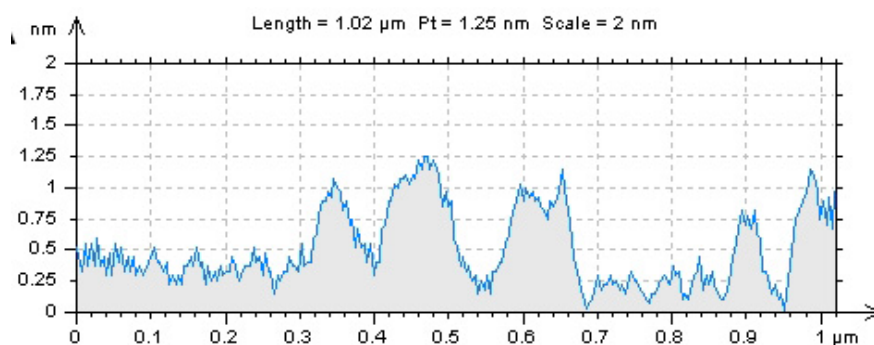


Figure 3.5 Profile extraction analysis of GO.

While its lateral dimensions can range from a few nanometers up to hundreds of micrometers, which is common for colloidal particles. Figure 3.6 depicts topography (A) and phase contrast (B) of graphene oxide prepared by placing a droplet of solution on to mica and evaporating the aqueous solvent. One can observe the sheet-like structure of GO with a varying lateral size.

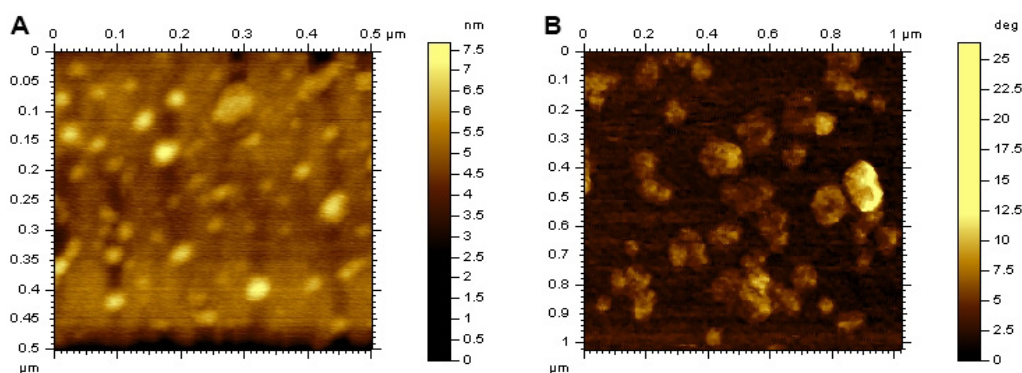


Figure 3.6 2D images of graphene oxide (A) topography and (B) phase contrast.

3.2.2 Aggregation of GO in electrolyte solution

One of the potential applications of GO is its use as a carrier in drug delivery. The large surface area, sp^2 hybridized aromatic carbon rings and functionalization potential allow for GO to be an ideal molecule for transporting therapeutic agents into the body. A significant concern regarding the use of GO in biological applications is aggregation. It has been shown that GO has a tendency to aggregate in an electrolyte solution, leading to decreased bio-functionalization and cellular uptake efficiency.³²

GO in aqueous phase in the absence of electrolytes shows very strong dispersion and solubility due to sufficient ionization from charged carboxylic acid groups which circumvent the molecule. However, when salt is present, such as is in physiological

buffers, counter-ions rapidly surround GO and reduce overall molecular charge. The direct result is a nonionic planar molecule with sufficient aromatic carbon rings to cause stacking due to π - π interactions.

3.2.3 Interaction between GO and Pluronic F-127

There are two proposed methods to prevent GO aggregation in an electrolyte solution, covalent attachment of a blocker or non-covalent, steric based blocker. Herein we report significant progress in aggregation prevention via non-covalent means. It is hypothesized that by using Pluronic F-127 as an additive in a solution of GO, the GO remains dispersed and its aggregation is prohibited. The first step is to ensure an interaction between the two molecules. Based on the AFM images in Figure 3.6, it can be assumed that there is an affinity for the two to network.

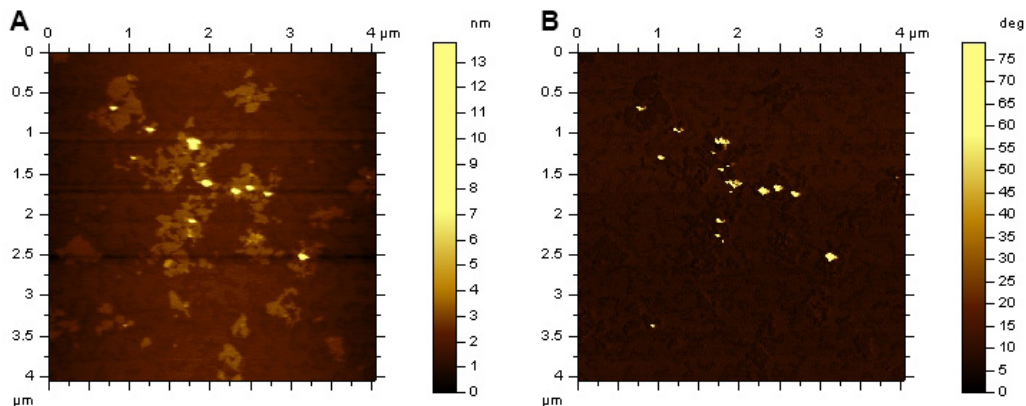


Figure 3.7 2D topography (A) and phase contrast (B) of a 2:1 solution of GO to Pluronic F-127.

Pluronic F-127 can easily be identified as the bright pixels in the phase contrast images, furthermore, it can be shown that the polymer only exists where GO is present based on the topography image.

Due to interactions between the central hydrophobic segment of Pluronic F-127 (See Figure 3.1) and the hydrophobic basal plane of GO, the copolymer and nanomaterial

form a complex. Pluronic F-127 cannot be found anywhere GO is not present. Based on the hydrophobic interaction hypothesis, one would expect Pluronic F-127 to assemble on both sides of the basal plane of GO. Figure 3.8 depicts the profile extraction analysis of GO and Pluronic at a ratio of 2:1. Judging from the heights in Figure 3.8b and from the literature values for Pluronic F-127 height, it can be assumed that Pluronic F-127 is non-covalently bound to both sides of GO (5 nm + 1 nm + 5 nm). Figure 3.9 depicts a three-dimensional rendering of the varying heights present in the sample.

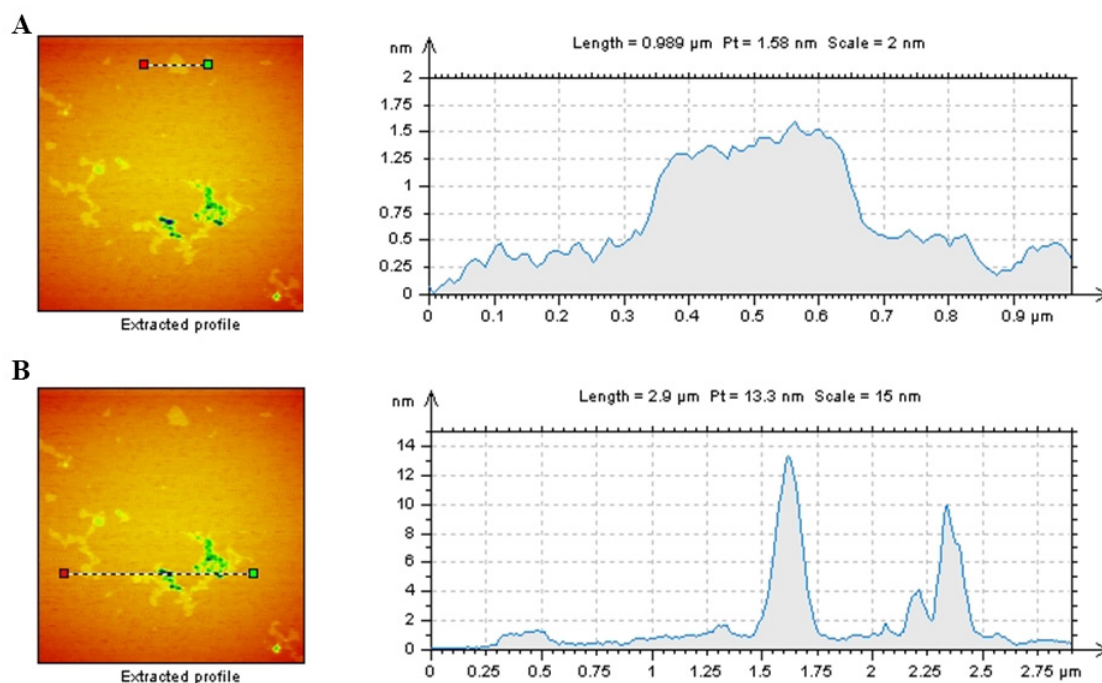


Figure 3.8 Profile extraction analysis of GO / Pluronic F-127 mixture (2:1). GO (A), GO / Pluronic F-127 interaction (B).

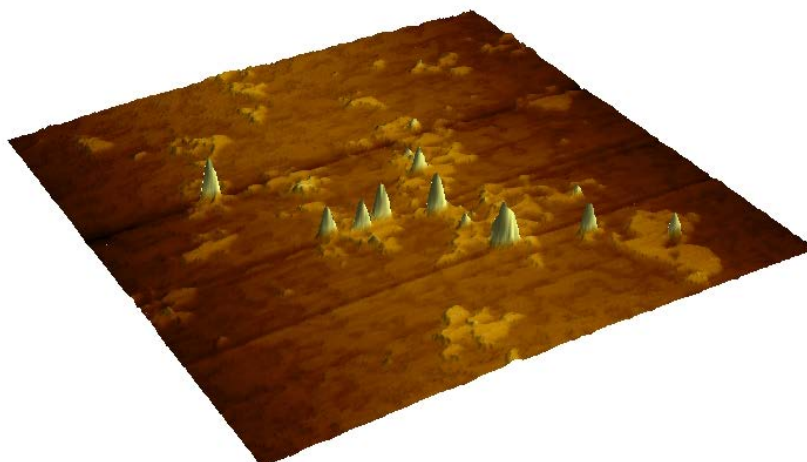


Figure 3.9 3D topography of GO / Pluronic F-127 mixture (2:1).

In conclusion, the interaction between GO and Pluronic F-127 can be confirmed. There is an affinity for the two to non-covalently link. Additionally, due to the interaction, GO has a counter effect on the copolymer, it prevents self-assembly. Based on this information, one can conclude that the hydrophobic interaction between GO and Pluronic F-127 is stronger, and therefore supersedes, the hydrophobic interaction between Pluronic and itself. Furthermore, the evidence suggests that the use of a non-covalent additive, such as Pluronic F-127 which has great biocompatibility, would prevent aggregation of GO in an aqueous, electrolytic solution, thereby allowing increased efficiency in biological applications.

3.3 (ZnS)-CdSe quantum dots

3.3.1 Background

The search for high quality, efficient semiconducting nanocrystals has led to the innovation and optimization of quantum dots. Quantum dots are semiconducting nanoparticles that have a size of 1 – 10 nm in all three dimensions.³³ The final size of the particles is dependent on synthetic conditions, which allows for easy tunability as the

optical properties are directly related to the size of the quantum dots. One particular application of quantum dots is their use in solar cells as a means of harvesting alternative energy from the sun efficiently. Short band gap semiconductors like these can be used to absorb light energy and convert it into a photocurrent when paired with an electrode surface onto which they are attached in an orderly array. Because quantum dots can be easily tuned for a particular size during synthesis, one can vary the band energies in order to modulate the vector charge transfer across differently sized particles. Therefore one can drive the energetics to more favorable conditions in order to allow for electron injection from the quantum dots into the electrode surface for conduction.³⁴ Consequently, being able to accurately characterize these particles for size distribution becomes very important to gauging semiconducting efficiency for potential applications. Herein, the size characterization of (ZnS)-capped CdSe quantum dots with reported diameters of 2 nm will be studied solely using AFM topographic techniques.

3.3.2 Size characterization

By utilizing the sensitive morphological technique of AFM, we are able to obtain highly detailed images of (ZnS)-capped CdSe quantum dots (See Figure 3.9). Based on the profile extraction in Figure 3.10, it can be noted that as the sample is dried on the slide, quantum dots within close proximity aggregate into large clumps. This data is further complicated due to the phenomenon of tip convolution, whereby the nominal radius of the tip is larger than the particle itself, thereby depicting a bloated lateral measurement. However, measurements on the z-axis are considered accurate down to <1 nm, and as quantum dots are considered spherical particles, the measured 2 nm heights can be attributed to 2 nm diameters.

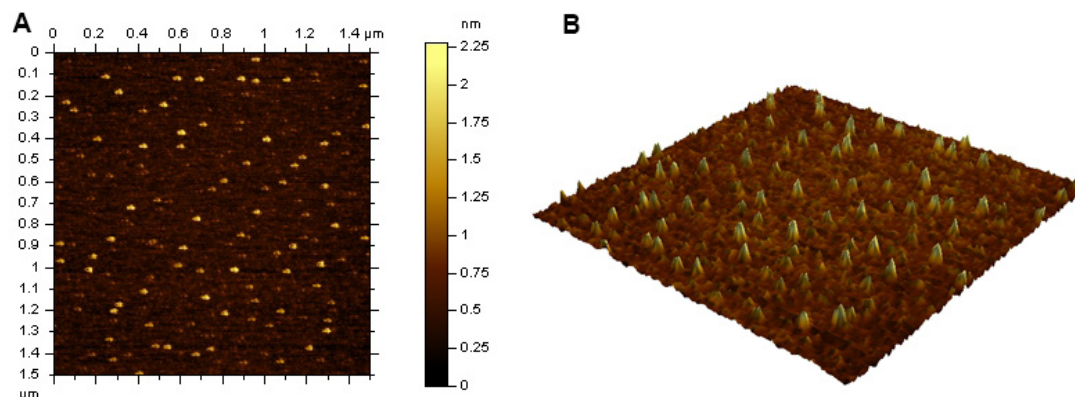


Figure 3.10 2D (a) and 3D (b) topography images of (ZnS)-capped CdSe quantum dots.

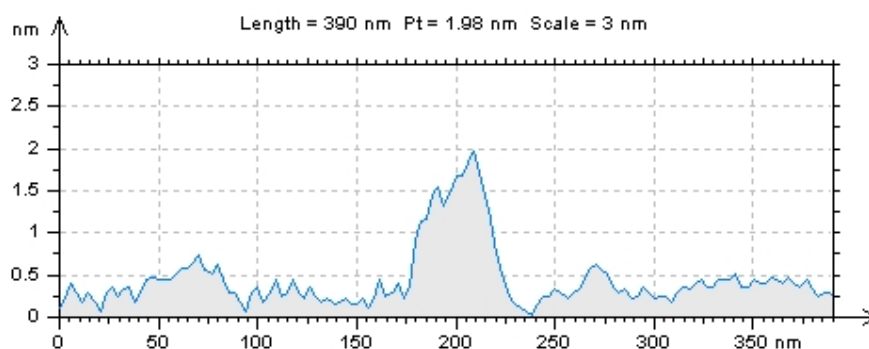


Figure 3.11 Profile extraction analysis of (ZnS)-capped CdSe quantum dots.

3.3.3 Size histogram

Furthermore, the powerful imaging software included with AFM is capable of calculating much more information based solely on the images taken. Figure 3.11 depicts a size histogram calculated from the topographic image in Figure 3.9a. One can see that the majority of particles range between roughly 1.70 and 2.08 nm, giving a very small size distribution, which when in effect, will increase efficiency of conduction when applied.

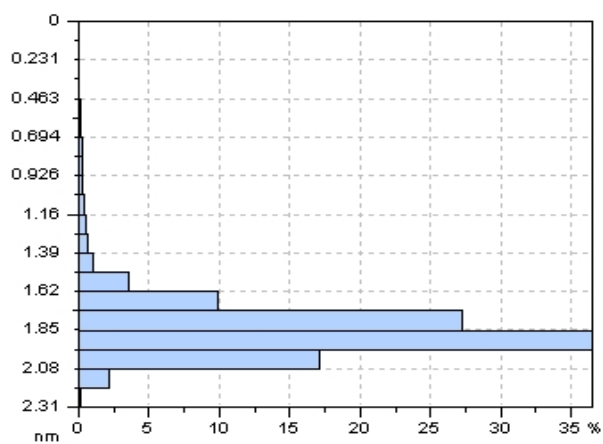


Figure 3.12 Histogram of quantum dot sizes derived from AFM imaging.

Chapter 4. Peptide Binding

4.1 Background

The search for efficient and inexpensive green catalysts has been growing significantly as serious environmental and energy concerns begin to emerge. Traditional catalysts, both homogenous and heterogeneous, have been produced at the industrial scale for some time now; however, the implications of producing toxic waste materials in the process are weighing heavily on the field. Desirable traits in a green catalyst include aqueous medium, room temperature reactions and low catalyst loadings. Metallic palladium nanoparticles have been hypothesized as a practical alternative, particularly in the catalytic formation of C-C bonds, such as in Stille or Suzuki coupling.³⁵ However, such reactions still require high activation temperatures (70 - 100 °C) and organic solvents, such as toluene.³⁶

In contrast, another approach based on producing biomimetic palladium nanoparticles stabilized by an aqueous soluble peptide has recently been introduced.³⁷ The peptide of choice is called Pd4, it consists of twelve amino acids, two of which are histidine residues. It is hypothesized that these histidines, located at positions 6 and 11, bind palladium in a pinched arrangement, leading to open interaction sites between the metal and molecules in solution, ideal for catalysis. In fact, C-C bond formation occurs within 24 h, at room temperature with minimum catalyst loading. However, the A6 peptide, a mutant form of Pd4 sans one of the two histidine residues, appears to be five-fold more efficient. It should also be noted that both peptides provided identically sized nanoparticles. Herein, we utilize AFM to study the binding properties of Pd4 as well as

the mutant A6 on to a palladium surface to further understand the mechanism of catalysis.

4.2 Nature of binding

Prior to beginning experiments with QCM, it is important to characterize the palladium coated substrate. Figure 4.1 depicts the AFM topography and phase contrast of a freshly cleaned surface. As can be seen, the surface is indeed extremely flat. This is attributed to the cleaning process itself. As palladium is sputter coated onto the surface, it leaves an uneven topography. Upon treatment with a strong base and UV plasma radiation, any atoms that are nested both above and below the mean roughness are removed, leaving an atomically flat surface.

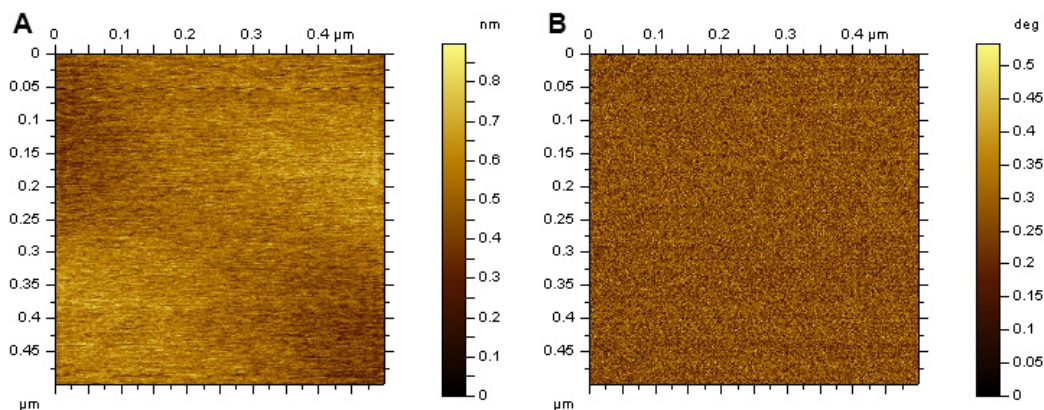


Figure 4.1 Topography and phase contrast of clean QCM substrate.

An interesting occurrence is observed after performing a control QCM experiment wherein ultrapure water alone is flowed over the cleaned surface. As can be seen in Figure 4.2a, the topography of the palladium coated surface no longer remains flat. Due to the chip being subjected to strong vibrations at its resonant frequency, atoms on the surface become dislodged in a process known as *pitting*, this results in a topography that resembles peaks and valleys with a depth range of 3-4 nm on the z-axis. It can be

assumed that due to the small size of the peptides in question (roughly 1 nm in length), differentiating binding locations from pitted locations will be incredibly difficult. In order to overcome this obstacle, we must take advantage of the benefits of phase contrast AFM.

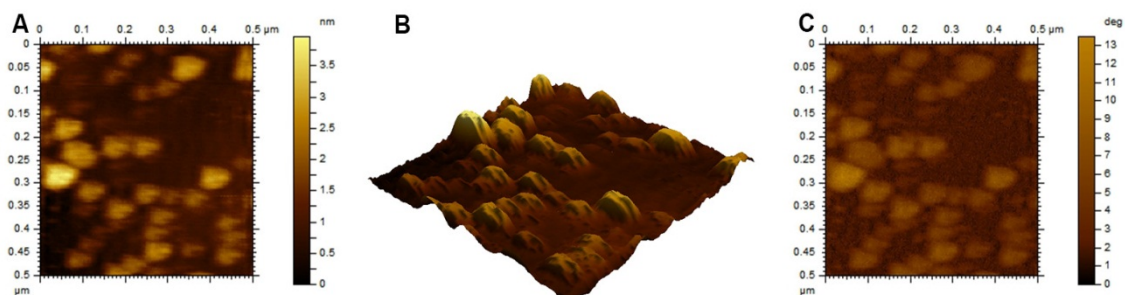


Figure 4.2 2D (A) and 3D (B) topography and phase contrast (C) of palladium coated chip after control QCM experiment.

As mentioned earlier, phase contrast is able to measure changes in surface ‘hardness’ through detecting adhesive and frictional forces as the tip oscillates. There is very little change of phase observable in our control QCM experiment (Figure 4.2c). Due to the fact that we see changes in topography where *pitting* occurs, the surface hardness still, however, remains the same. Therefore, due to the ‘soft’ nature of peptides, we expect to see significant change in phase contrast where binding occurs.

Figure 4.3 shows the AFM topography images of the Pd4 and A6 peptides run at the three different concentrations. Based on these images, it is clear that the use of topography alone will be of no merit in the binding discussions. In the cases of Figure 4.3a and 4.3f, we may be able to locate some peptide on the surface; however, these images in no way indicate all bound peptides.

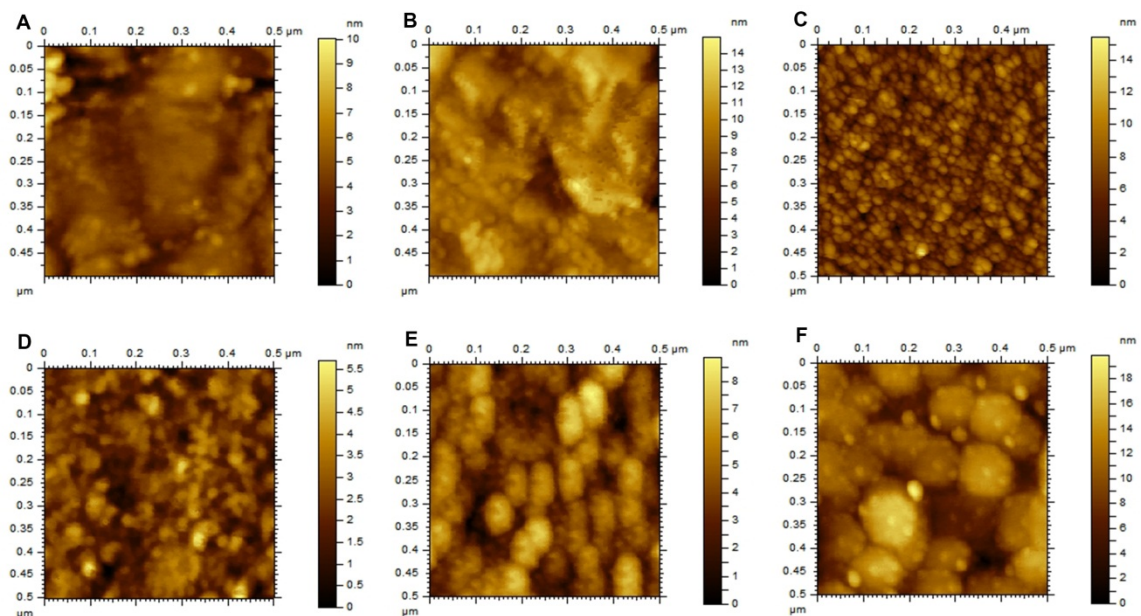


Figure 4.3 Topography of Pd4 (top) and A6 (bottom) peptides at varying concentrations: (A,D) 5 $\mu\text{g/ml}$, (B,E) 10 $\mu\text{g/ml}$, (C,F) 15 $\mu\text{g/ml}$.

However, upon studying the phase contrast images of the same samples (See Figure 4.4), evidence of complete peptide binding becomes clear and quantified.

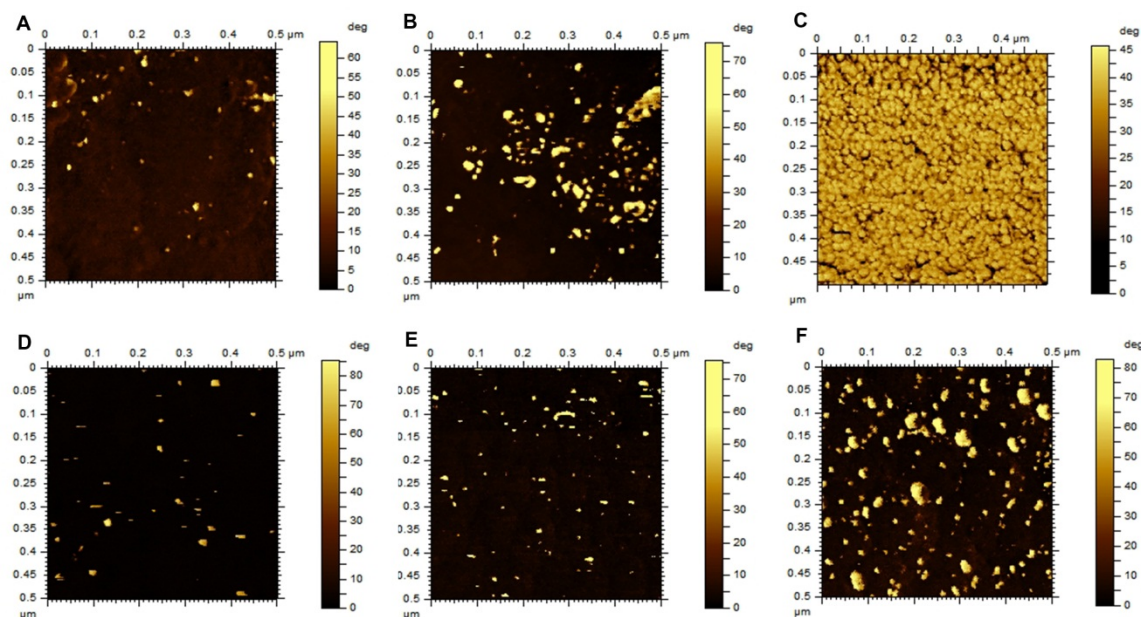


Figure 4.4 Phase contrast images of Pd4 (top) and A6 (bottom) peptides at varying concentrations: (A,D) 5 $\mu\text{g/ml}$, (B,E) 10 $\mu\text{g/ml}$, (C,F) 15 $\mu\text{g/ml}$.

By studying the phase contrast analysis a clear correlation between peptide and binding profile can be observed. As we see in Figure 4.4, the Pd4 peptide, with two histidine residues, binds much more readily than the A6 mutant peptide which contains only one histidine residue. This finding, further supports the hypothesis that histidine truly is the obligatory link involved in biomineralization of palladium nanoparticles.

The AFM images provide interesting evidence regarding the mechanism of catalysis and an explanation for the difference in catalytic activity between the two peptides. QCM adsorption of Pd4 peptide at the highest concentration seems to saturate the surface, it is apparent that the visible peptide ‘islands’ that are formed are separated by small clefts that measure between 3 – 10 nm in width (See Figure 4.5). Although, these crevices are large enough to reveal enough of the catalytic Pd surface for reactivity, the A6 peptide binding results in much greater available surface area, resulting in greater catalytic activity.

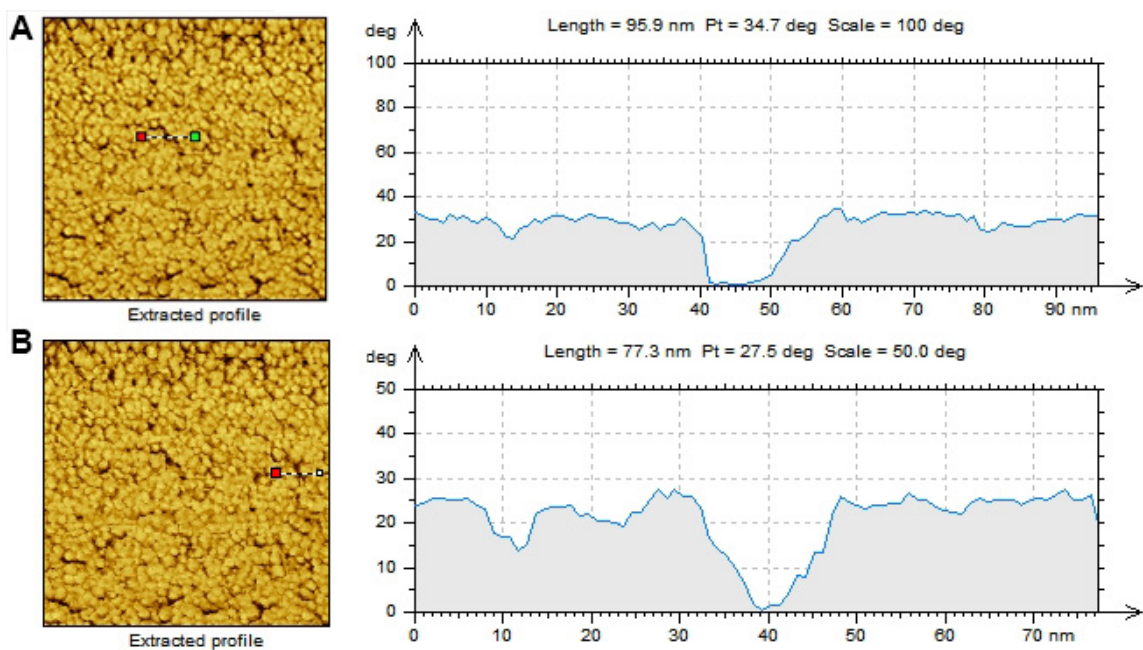


Figure 4.5 Profile extraction analysis of Pd4 peptide at 15 µg/ml taken with phase contrast AFM.

Chapter 5. Amyloid Fibril Formation

5.1 Background

Recent developments in human diseases caused by insoluble extracellular deposits of proteins have led to a shift in biochemical research over the past few decades. These deposits, called amyloid fibrils, consist of normally soluble proteins which have accumulated in the extracellular space of various tissues and are roughly 10 nm in diameter.³⁸ The exact mechanism of fibril formation is not known, however, it is widely believed that they are formed by protein mis-folding and self-assembly into highly ordered fibrillar assemblies rich in β -sheet secondary structure.³⁹ More specifically, fibrillation occurs under conditions where proteins are partially or completely destabilized or unfolded. Following this, the protein shifts into an alternative packing conformation which reduces its surface-accessible area, saturates hydrogen bonding, and reaches an alternative 'nonnative' global minimum in free energy.⁴⁰ The formation of amyloid aggregates is characteristic of many neurodegenerative diseases such as Alzheimer's, Parkinson's and Huntington's disease. Herein, the fibrillation of human insulin, representing type-2 diabetes, will be studied using the AFM methodology.

5.2 Human Insulin

In order to study the growth of insulin fibrils, it is important to first understand the conditions necessary to facilitate artificial fibrillation. *In vitro* fibril formation has been found to be optimal under relatively extreme conditions. It should be noted that insulin amyloid plaques are commonly found *in vivo* primarily in pancreatic tissue under physiological conditions, however, for the sake of experimental demonstration, higher temperatures and lower pH were used, specifically 65 °C and pH of 2. Additionally, due

to the hydrophilic nature of proteins, the substrate for all insulin images was mica, freshly cleaved prior to each sample deposition.

Figure 5.1a depicts human insulin prior to incubation. At this point, the human insulin is at its most naturally folded state. The AFM image represents typical characteristics of a protein sample, i.e. large bundles or islands of aggregates with no uniform or ordered structure. It is important to understand that although the protein is aggregated, no denaturing has occurred. After 5 h of incubation (Figure 5.1b), the majority of larger protein ‘islands’ are no longer visible, instead smaller, more isolated fragments can be seen. This may signify a change in the folded state of insulin, administration of heat may have altered the configuration of the protein preventing large aggregates from remaining together. Although not conclusive evidence of the beginning stages of fibrillation, it is fair to say that an alteration of native folded state has occurred, changing the aggregation patterns of insulin. Insulin after 10 h of incubation (Figure 5.1c) displays similar characteristics as after 5 h of incubation. At this stage, no fibrillation has occurred, however, evidence has surfaced of potential variations in protein folding, which according to the hypothesis may signify the early stages of fibril formation.

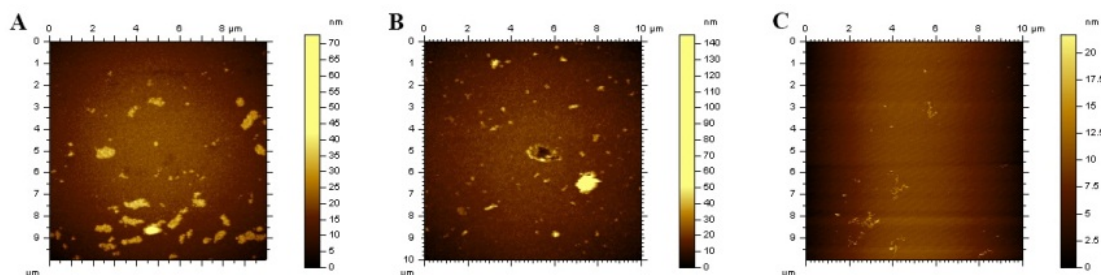


Figure 5.1 Topography of human insulin after 0 (A), 5 (B) and 10 h (C) incubation on mica.

Figure 5.2 follows the progress of insulin incubation to 14 (A), 17 (B) and 20 h (C). Although difficult to confirm, after 14 h, the first signs of true fibrillation occur

(Figure 5.2a). We begin to see small ‘string’ like structures appear at the edge of the image. These structures bear no resemblance to insulin in its native folded state. In Figures 5.2b, 5.2c and 5.2d, fibril growth is realized. At these stages in incubation, morphological differences in fibril formation can clearly be observed.

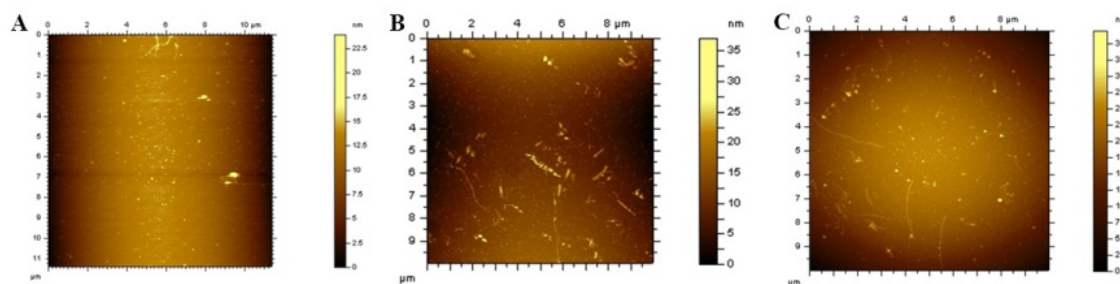


Figure 5.2 Topography of human insulin after 14 (A), 17 (B) and 20 h (C) incubation on mica.

Finally, after incubation for 24 h, we observe total and complete fibril growth. Figure 5.3 depicts fully developed insulin amyloid fibrils. Based on the profile extraction analysis described in Figure 5.4, the organized structures maintain a 10 nm diameter, consistent with literature values. It appears as though upon incubation, human insulin begins an unfolding process, typical of all proteins, however the denaturation continues by ordered aggregation into fibril like structures. These large structures maintain strong stability and are considered to be at an alternative ‘nonnative’ global free energy minimum. With the powerful topographic tools inherent within AFM, we are able to witness the morphological changes occurring in human insulin incubated over time.

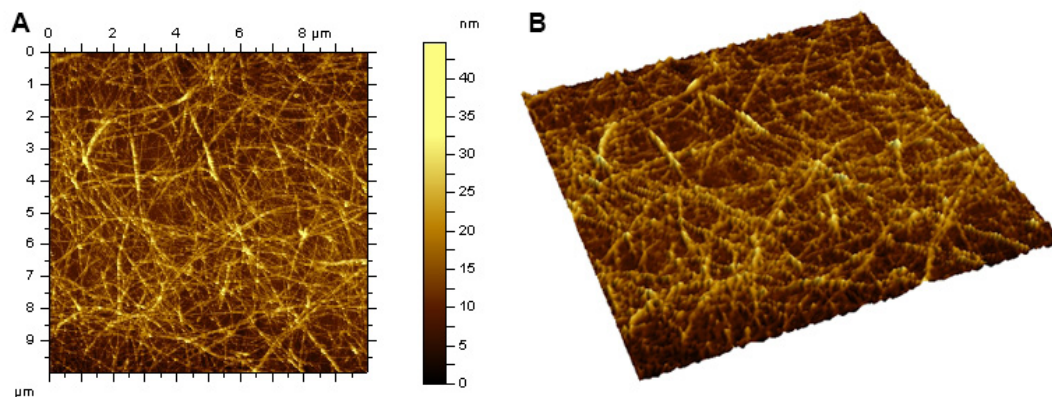


Figure 5.3 2D (A) and 3D (B) topography of human insulin after incubation for 24 h.

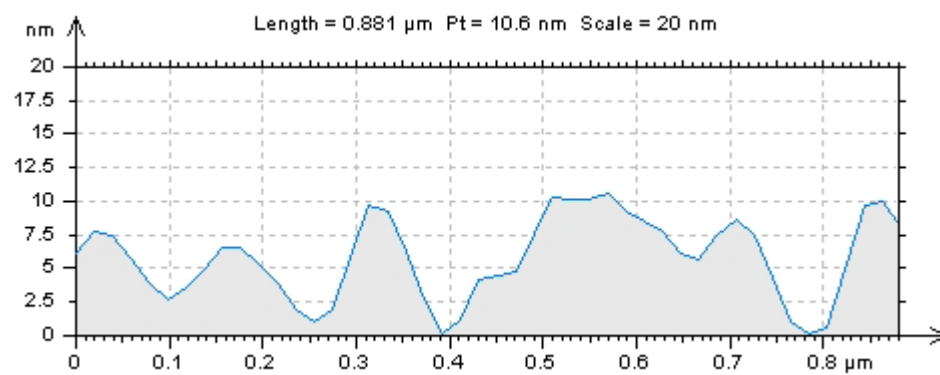


Figure 5.4 Profile extraction analysis of human insulin fibrils after 24 h incubation.

Chapter 6. Future Work

The work reported in this thesis describes various topographical techniques that are used to help characterize and understand nanomaterials and biomolecules. There are aspects of the work reported that I would like to expand on further. For example, additional images need to be taken with regards to varying ratios of graphene oxide and Pluronic F-127 to provide additional understanding and evidence of the hypothesized interaction between the two molecules. Furthermore, with regards to the peptide binding experiments, additional mutant peptides will be studied to provide more information regarding the relationship between peptide sequence and catalytic activity. Finally, additional proteins related to amyloid fibril formation will be studied in order to solidify the hypothesized mechanism and to demonstrate its validity on multiple proteins. Understanding topography can be a powerful tool in helping to accurately characterize molecules and elucidate mechanisms. However, AFM is capable of performing many more functions that expand its potential applications greatly. Another major application, besides imaging, is force spectroscopy, which is the direct measurement of tip-sample interaction forces. These measurements can be used to measure such things as atomic bonding and van der Waals interactions. The most notable transition from the work reported in this thesis is to utilize force spectroscopy in the measurement of the mechanical properties of both nanomaterials and biomolecules. Potential future work related to force spectroscopy AFM could prove to be extremely useful when used in conjunction with topographic data.

References

1. Binnig, G.; Quate, C. F.; Gerber, Ch. *Phys. Rev. Lett.* **1986**, 56, 930-933.
2. Binnig, G.; Rohrer, H. *Surf. Sci.* **1982**, 126, 236-244.
3. Chen, J. *Introduction to Scanning Tunneling Microscopy*. Oxford University Press, New York, NY, **1993**.
4. Agilent Technologies Atomic Force Microscopy User Manual, **2009**.
5. Curie, J.; Curie, P. *Bulletin de la Société minéralogique de France*. **1880**, 3, 90.
6. Chen, X.; Roberts, C. J.; Zhang, J.; Davies, M. C.; Tendler, S. J. B. *Surf. Sci.* **2002**, 519, L593-L598.
7. Pang, D.; Chasovskikh, S.; Cohen, J.S.; Obcemea, C.; Dritschilo, A. *Int. J. Cancer*. **2000**, 90, 68-72.
8. Magonov, S.; Reneker, D. *Annu. Rev. Mater. Sci.* **1997**. 27, 175-222.
9. Matlis, S.; Edgar, R. *Surf. Interface Anal.* **1999**. 27, 374-378.
10. <http://www.nanowerk.com/spotlight/spotid=4876.php>
11. Agilent Technologies Application of Atomic Force Microscopy on Particle Characterization, **2008**.
12. Drake, B.; Prater, C. B.; Weisenhorn, A. L.; Gould, S. A.; Albrecht, T. R. *Science*. **1989**, 243, 1586-1589.
13. Hoh, J. H.; Lal, R.; John, A.; Revel, J. P.; Arnsdorf, M. F. *Science*. **1991**, 253, 1405-1408.
14. de Jager, M.; van Noort, J. *eLS*. **2007**.
15. <http://www.jpik.com/substrates-in-general-mica.443.en.html>
16. Kindt, J. H.; Sitko, J. C.; Pietrasanta, L. I.; Oroudjev, E.; Becker, N.; Viani, M. B.; Hansma, H. G. *Methods Cell Biol.* **2002**, 68, 213-229.
17. da Silva, L. P. *Protein Peptide Lett.* **2002**, 9, 117-125.
18. Venkatesh V.C.; Inasaki, I.; Toenshoff, H. K.; Nakagawa, Y.; Marinescu, I. *Annals of the CIRP*. **1995**, 44, 611-618.
19. Delhaes, P. *Graphite and Precursors*. CRC Press, **2001**.
20. Shao, Z.; Mou, J.; Czajkowsky, D. M.; Yang, J.; Yuan, J-Y. *Adv. Phys.* **1996**, 45, 1-86.
21. Amrein, M.; Müller, D. J.; *Nanobiology*. **1999**, 4, 229-256.

22. Höök, F.; Rodahl, M.; Brzezinski, P.; Kasemo, B. *Langmuir*. **1998**, 14, 729-734.
23. Murray, B. S.; Deshares, C. J. *J. Coll Interf. Sci.* **2000**, 227, 32-34.
24. Dickerson, M. B.; Jones, S. E.; Cai, Y.; Ahmad, G.; Naik, R. R.; Kroger, N.; Sandhage, K. H. *Chem. Mater.* **2008**, 20, 1578-1584.
25. Skaat, H.; Belfort, G.; Margel, S. *Nanotechnology*. **2009**, 20, 1-9.
26. <http://www.sigmaaldrich.com/catalog/product/sigma/p2443?lang=en®ion=US>
27. Geim, A. K.; Novoselov, K. S. *Nature Materials*. **2007**, 6, 183-191.
28. Zu, Z-S.; Han, B-H. *J. Phys. Chem. C*. **2009**, 113, 13651-13657.
29. Kaplan, J. H.; Passow, H. *J Membr. Biol.* **1974**, 19, 179-194.
30. Gao, J; Zhang, W.; Huang, P.; Zhang, B.; Zhang, X.; Xu, B. *J. Am. Chem. Soc.* **2008**, 130(37), 12201-12203.
31. Hong, B. J.; Compton, O. C.; An, Z.; Eryazici, I.; Nguyen, S. T. *ACS Nano*. **2012**, *in press*.
32. Stankovich, S.; Dikin, D. A.; Piner, R. D.; Kohlhaas, K. A.; Kleinhammes, A.; Jia, Y.; Wu, Y.; Nguyen, S. T.; Ruoff, R. S. *Carbon*. **2007**, 45 1558-1565.
33. Weller, H. *Adv. Mater.* **1993**, 5, 88-95.
34. Kongkanand, A.; Tvrdy, K.; Takechi, K.; Kuno, M.; Kamat, P. *J. Am. Chem. Soc.* **2008**, 130(12), 4007-4015.
35. Astruc, D. *Inorg. Chem.* **2007**, 47, 1884-1894.
36. Stille, J. K. *Angew. Chem. Int. Ed. Engl.* **1986**, 25, 508-524.
37. Pacardo, D. B.; Sethi, M.; Jones, S. E.; Naik, R. R.; Knecht, M. R. *ACS Nano*. **2010**, 3, 1288-1296.
38. Sunde, M.; Blake, C. C. *Q. Rev. Biophys.* **1998**, 31, 1-39.
39. Stefani, M.; Dobson, C. M. *J. Mol. Med.* **2003**, 81, 678-699.
40. Gazit, E. *Angew. Chem. Int. Ed. Engl.* **2002**, 41, 257-259.